



Published in final edited form as:

Nanomedicine. 2012 August ; 8(6): 941–950. doi:10.1016/j.nano.2011.11.011.

Multifunctional Nanoplatfoms for Fluorescence Imaging and Photodynamic Therapy Developed by Post-loading Photosensitizer and Fluorophore to Polyacrylamide Nanoparticles

Anurag Gupta, BS¹, Shouyan Wang, PhD², Paula Pera, MSc¹, K.V.R. Rao, PhD¹, Nayan Patel, BA¹, Tymish Y. Ohulchanskyy, PhD³, Joseph Missert, MSc¹, Janet Morgan, PhD⁴, Yong-Eun Koo-Lee, PhD², Raoul Kopelman, PhD^{2,*}, and Ravindra K. Pandey, PhD^{1,*}

¹PDT Center, Roswell Park Cancer Institute, Buffalo, NY 14263

²Department of Chemistry, University of Michigan, Ann Arbor, MI 48109-1055

³Institute of Lasers, Photonics and Biophotonics, University of Buffalo, NY 14221

⁴Department of Dermatology, Roswell Park Cancer Institute, Buffalo, NY 14263

Abstract

We report a novel post-loading approach for constructing a multifunctional biodegradable polyacrylamide (PAA) nanoplatfom for tumor-imaging (fluorescence) and photodynamic therapy (PDT). This approach provides an opportunity to post-load the imaging and therapeutic agents at desired concentrations. Among the PAA nanoparticles, a formulation containing the photosensitizer, HPPH [3-(1'-hexyloxyethyl)pyropheophorbide-a], and the cyanine dye in a ratio of 2:1 minimized the undesirable quenching of the HPPH electronic excitation energy due to energy migration within the nanoparticles and/or Förster (fluorescence) resonance energy transfer (FRET) between HPPH and cyanine dye. An excellent tumor-imaging (NIR fluorescence) and phototherapeutic efficacy of the nanoconstruct formulation is demonstrated. Under similar treatment parameters the HPPH in 1% Tween 80/5% aqueous dextrose formulation was less effective than the nanoconstruct containing HPPH and cyanine dye in a ratio of 2 to 1. This is the first example showing the utility of the post-loading approach in developing a nanoconstructs for tumor-imaging and therapy.

Keywords

Near-Infrared Fluorescence Imaging; Photodynamic Therapy; Post-Loading; Polyacrylamide Nanoparticles

© 2011 Elsevier Inc. All rights reserved.

To whom correspondence should be addressed: Ravindra K. Pandey (ravindra.pandey@roswellpark.org), Raoul Kopelman (kopelman@umich.edu).

Publisher's Disclaimer: This is a PDF file of an unedited manuscript that has been accepted for publication. As a service to our customers we are providing this early version of the manuscript. The manuscript will undergo copyediting, typesetting, and review of the resulting proof before it is published in its final citable form. Please note that during the production process errors may be discovered which could affect the content, and all legal disclaimers that apply to the journal pertain.

Conflict of Interest: A part of the technology presented in this manuscript is licensed to Photolitec, LLC, USA.

Supporting Material: Detailed methods for synthesizing blank NPs and post-loading procedures for optical imaging, SEM, DLS and release kinetics.

Background

Both cancer detection and treatment depend on selective delivery of appropriate agents to the malignancy. Photodynamic therapy (PDT), a relatively new modality for the treatment of a variety of oncological, cardiovascular, dermatological and ophthalmic diseases, is based on the preferential localization of photosensitizing molecules, (photosensitizers, PS) in target tissues.¹⁻⁵ Upon light activation, the PS produces reactive singlet oxygen⁵ which damages tumor cells and neovasculature, and also initiates antitumor inflammatory and immune responses.^{6,7} We and others have developed relatively tumor-avid PS which selectively accumulate in tumor, and these molecules have been used to carry optical, PET and MR imaging agents to the tumor sites.^{8,9} However, the tumor selectivity of current PS is not always adequate. Approaches that link PS to antibody fragments or receptor ligands have been disappointing because the number of required PS/cell generally is greater than the number of antigen or receptor binding sites.¹⁰ Conversely, the imaging agent carrying capacity of the individual PS molecules is limited.

Nanotechnology platforms potentially can deliver large numbers of PS and/or imaging agents.¹¹ Nanoparticles (NP) are uniquely promising in that (i) their hydrophilicity and charge can be altered; (ii) they possess enormous surface area which can be modified with functional groups possessing a diverse array of chemical and biochemical properties, including tumor-selective ligands; (iii) owing to their sub-cellular and sub-micron size, they can penetrate deep into tissues and are generally taken up efficiently by cells; (iv) since numerous universal strategies for the preparation of nanomaterials are already in place, PS-loaded nanoparticles can be made by numerous methods, such as covalent linkages, self assembly, etc..

We have recently shown that HPPH, developed in our laboratory¹²⁻¹⁷ and currently under Phase I/II clinical trials, when conjugated with certain cyanine dyes can be used for both fluorescence imaging and photodynamic therapy.^{18,19} The conjugate showed potential tumor imaging and PDT efficacy, but compared to the imaging dose the required therapeutic dose was 8-fold higher. Increasing the number of HPPH moieties in synthetic photosensitizer-cyanine dye (PS-CD) conjugates did not minimize the therapeutic dose.¹⁸ We envision the comprehensive development, characterization and validation of multifunctional nanovector platforms that can deliver tumor-avid therapeutic photosensitizers that only become active (and toxic) when illuminated by specific wavelengths of light, and, in addition, carry one or more imaging agents; these nano-platforms thus could enable both diagnosis and image guided therapy.

Among the nanoparticles, hydrogel polyacrylamide (PAA) in which the monomeric units are linked together with ester bonds have been of particular interest due to their biocompatibility/biodegradability and low toxicity.^{20a,b} Using biodegradable polymer based nanoparticles (NPs) avoids multi-step synthesis and has numerous advantages including the ability to create water soluble formulations with desired pharmacokinetic properties, capable of delivering a high payload of the multiple agents (therapeutic PS and imaging agents) to tumors, increased photostability of photoactive agents and fluorophores, and the ability to modify the surface of the NP for conjugation to a variety of biomolecules. NPs and other macromolecular objects can passively target the tumor interstitium, via the “Enhanced Permeability and Retention” (EPR) effect due to the leaky vascular system in tumors.^{21a,b} In addition, the poor lymphatic drainage system in tumors causes fluid retention in the tumor interstitial space, which helps to retain polymeric nanoparticles and other macromolecular objects in the tumor compared to normal tissue.^{21a,b} For these reasons, NPs are a promising means for delivering therapeutic and other molecular agents to tumors.

Because NPs could deliver a high payload of the drug to tumor, we investigated the use of a PAA-based nanoconstructs for delivering both the near-infrared (NIR) cyanine dye (CD) fluorophore and the red-light absorbing photosensitizer HPPH. The release of the desired imaging and therapeutic agents may also be controlled by creating a nanoparticle that is pH or temperature sensitive, or by modifying the pores of the NP matrix.²² In a parallel study²³ we encapsulated the PS within polymeric NPs, but the retention efficiency was low, therefore a large concentration of NPs was required to achieve the desired therapeutic dose. To increase the retention of the PS within the NP, we decided to form the NPs first and then load the PS into the porous PAA-NPs. This novel loading approach of the desired agents was termed “*post-loading*”. In this procedure, both HPPH (phototherapeutic agent) and the cyanine dye (NIR fluorescence imaging agent) moieties were highly retained in the NPs (confirmed by release kinetics) and provided constructs for non-invasive detection of tumors and delineation of the tumor margins by NIR fluorescence imaging.

Fluorescence imaging is a non-invasive and non-ionizing imaging technique that requires only nanomoles of fluorophores for contrast enhancement.^{24,25} The NIR spectral range (~650 – 950 nm) is known as the “biological window” for optical imaging since light absorption due to water, deoxygenated hemoglobin and oxygenated hemoglobin is minimized in this region, as well as tissue autofluorescence and light scattering.^{11b,c}

In this study, we compared the photosensitizing and NIR fluorescence imaging potential of several biodegradable PAA nanoparticle formulations, in which the HPPH and CD moieties were post-loaded at a 2 to 1 and a 4 to 1 ratio, respectively. These formulations were significantly different in tumor uptake, in pharmacokinetics and in *in vivo* imaging and PDT efficacy.

Methods

Materials

Human Serum Albumin, Tween-80 and dimethyl sulfoxide (DMSO) were purchased from Sigma-Aldrich. Bovine Calf Serum (BCS) was purchased and dPBS (pH 7.4, 1x, without calcium and magnesium) were purchased from Cellgro. Ethanol (200 proof) was purchased from Pharmco-Aaper. All solutions were prepared with 18 MO water purified by a Millipore Milli-Q Advantage A10 water purification system. 30 and 100 kDa Amicon Ultra-15 and Ultra 4 centrifuge filters were purchased from Fisher Scientific.

Animal Studies: All animal studies were performed following the animal protocol guidelines approved by Institutional Animal Care and Use Committee (IACUC).

Synthesis of blank nanoparticles—The PAA nanoparticles were prepared by following our previous report with slight modifications (See “Supporting Material Information” for the synthesis).²⁶

Post-Loading of the Photosensitizer 1, and the cyanine dyes 2, and 3 to blank AFPAA to create nanoconstructs 4, 5, 6, 9, and 10—In brief, 10 mg of lyophilized PAA NPs were suspended in 1 mL of 1% Tween-80 / water solution and to this solution 10 μ L of **1**, **2**, or **3** (20 mM in DMSO) is added and magnetically stirred at a constant rpm for 2 hours. The NPs were centrifuge filtered in a 30 kDa Amicon Ultra-15 centrifuge filter for 30 minutes at 5,000 RPM and then the NPs were reconstituted with water. The nanoparticles were syringe filtered with a 0.2 μ m regenerated cellulose syringe filter. Nanoformulation **9** and **10** were created by mixing nanoconstruct **1** and **3** such that the molar ratio of **1** to **3** was 2:1 and 4:1, respectively. The NPs are stored at 4° C until further use. For details see “Supporting Material Information”.

Post-Loading of the photosensitizer 1 and the cyanine dye 3 to blank AFPAA to create nanoconstructs 7 and 8—Upon measuring the concentration of PS 1 in nanoconstruct 6, cyanine dye 3 in DMSO (20 mM) was added such that the molar ratio of PS 1 to cyanine dye 3 was either 2:1 or 4:1. Once cyanine dye 3 was added, the procedure is the same as for post-loading, PS 1 or cyanine dye 2 and 3. For detailed procedure see the "Supporting Material Information".

Release Kinetics Procedure—The *in vitro* release profile of the photosensitizer 1, and the cyanine dye 3 in nanoconstructs/formulations 5–10 was measured. The NPs from all formulations were suspended in a 1% human serum albumin (HSA) – water solution and immediately the absorbance value for the HSA/nanoconstruct solution was measured spectrophotometrically. To measure the release of the photosensitizer 1 and/or the cyanine dye 3 from the NP, the NP solution is centrifuge filtered in a 100 kDa Amicon ultra-4 centrifugation filter for 20 minutes at 4,000 RPM. The absorbance of the PS or fluorophore in the filtrate was spectrophotometrically measured (filtrate 1). The NPs in the retentate were reconstituted to the original volume with 1% HSA and re-centrifuge filtered (filtrate 2) and measured spectrophotometrically. The amount of 1 and/or 3 retained by the NP was confirmed by measuring the absorbance of the retentate upon reconstitution to the original volume with 1% HSA. If the sum total of all filtrates and the retentate is less than 90% of the stock value for either chromophore then ethanol is added to the centrifuge filter to measure what had adsorbed to the filter. These measurements were taken immediately post-addition of the nanoconstructs in a 1% HSA solution, 4 and 24 hours post addition of the nanoconstructs in the 1% HSA solution. Additionally, the release of PS 1 and cyanine dye 3 in nanoconstruct 7 was measured in 25% bovine calf serum (BCS) at 37° C. The procedure followed for the release of the PS/fluorophore in 25% BCS was similar to that of 1% HSA, except that the measurements were taken at 4, 8, 12, and 24 h post-addition of nanoconstruct 7.

Optical Imaging Setup—The fluorescence imaging was conducted in accordance with a protocol approved by the Institutional Animal Care and Use Committee IACUC at Roswell Park Cancer Institute and the Guide for the Use of Laboratory Animals. BALB/c mice (3 mice/group) bearing subcutaneous Colon 26 tumors on the right shoulder were injected *i. v.* (tail-vein) with either cyanine dyes or nanoconstructs/formulations. For a detailed description of the groups of mice imaged along with the dose, see the "Supporting Material Information".

Absorbance, Fluorescence, and Singlet Oxygen Measurements—The absorbance measurements were performed on a Varian Cary-50 Bio UV-Visible spectrophotometer. The concentrations of the NP formulations were measured in ethanol utilizing 47,500, 200,000 and 207,455 L mol⁻¹ cm⁻¹ as the respective molar extinction coefficients of 1, 2, and 3.

A SPEX 270M spectrometer (Jobin Yvon) was used for acquisition of fluorescence emission spectra in the far red and NIR spectral ranges, utilizing the first output port equipped with an InGaAs photodetector (Electrooptical Systems Inc., USA). A diode-pumped solid-state laser (Verdi, Coherent) at 532 nm was the excitation source. Generation of singlet oxygen (¹O₂) was detected by its phosphorescence emission peaked at 1270 nm. The decays of this emission were acquired using the Infinium oscilloscope (Hewlett-Packard) coupled to the output of the Hamamatsu IR-PMT which is attached to the second output port of the SPEX 270M spectrometer. Nanoconstructs 5 – 8 in polystyrene cuvettes were placed in front of the entrance to the spectrometer. The emission signal was collected at 90-degrees relative to the exciting laser beam with the use of additional long-pass filters (a 950LP filter and/or a

538AELP filter) to attenuate the scattered light and fluorescence from the samples. A second harmonic (532 nm) from the nanosecond pulsed Nd:YAG laser (Lotis TII, Belarus) operating at 20 Hz was used as the excitation source for time-resolved measurements.

In-Vivo Photodynamic Therapy—Eight- to twelve-week-old BALB/cAnNCr mice (Jackson Laboratory, Bar Harbor, ME) were inoculated subcutaneously (s.c.) with 1×10^6 Colon 26 cells. When tumors reached 40–70 mm³, mice were injected *i.v.* (tail vein) with PS **1** (formulated in 1% Tween 80/D5W) or PAA nanoconstructs/formulations **6–10** suspended in water and further diluted in D5W. 24 hours post *i.v.* injection (dose of PS **1**: 0.47 μmol/kg), mice (BALB/c mice bearing Colon 26 tumors, 10 mice/group) were restrained in plexiglass holders and tumors were irradiated at 665 nm with a fluence and fluence rate of 135 J/cm² at 75 mW/cm², respectively, using a pumped argon-dye laser. The growth of tumors was measured two to three times per week and the mice were monitored for a total of 60 days post PDT treatment. When the tumor regrowth was >400 mm³, the mice were euthanized according to the guidelines of the institute approved animal protocol.

Results

Preparation of HPPH and Near Infrared Cyanine Dye Post-Loaded PAA NPs

In an ongoing SAR study with a series of cyanine dyes (CD), we modified IR820 **2** with limited imaging potential to a highly avid CD **3** in which the chloro-group of IR820 was replaced with a *p*-aminothiol functionality. CD **3** formulated in 1% Tween 80 / 5% dextrose was tumor avid, but the corresponding PAA formulation produced enhanced tumor contrast. On the other hand PS **1** (HPPH) and nanoconstruct **6** showed similar PDT efficacy with 40% tumor cure at a dose of 0.47 μmol/kg. Although the PAA formulation did not enhance the PDT efficacy at similar treatment parameters, it did show a markedly improved tumor-specificity (determined by fluorescence imaging).²³ Our objective was to prepare a single platform for imaging and therapy, therefore we investigated a synthetic approach in which the PS **1** was conjugated with **3**. The resulting product showed excellent tumor-imaging ability (dose: 0.3 μmol/kg), but the therapeutic dose was 8- to 10-fold higher. The low activity of the conjugate could be due to a part of the singlet oxygen produced by exposing the tumors with light was quenched by the CD, which reduced its activity and thus required a higher dose of the agent (HPPH-CD) for achieving efficacy similar to PS (HPPH) **1**. HPPH-CD conjugate also exhibited significant FRET, which indirectly correlates to singlet oxygen production, a key cytotoxic agent for PDT. In other words molecules with higher FRET should show reduced singlet oxygen production and PDT efficacy.

Therefore, for our present study we were interested in preparing a series of multifunctional PAA nanoplatfoms in which the PS and the CD molecules are post-loaded together in variable ratios or separately post-loaded (Figure 2, nanoconstructs **4–10**) and to investigate their tumor imaging and therapeutic potential. We anticipated that among all the nanoconstructs, the nanoformulation **10** in which PS and CD were separately post-loaded and then mixed in a ratio of 4 to 1 may show enhanced PDT response due to lower singlet oxygen quenching probability by the cyanine dye or the energy transfer between the two chromophores (PS and CD) which could result in higher singlet oxygen production and improved long term tumor cure.

Characterization of PAA nanoparticles: Size, Dispersion, and Release Kinetics

To characterize the size and dispersity of the nanoparticles, dynamic light scattering (DLS) and scanning electron microscopy (SEM) was utilized. The DLS showed a mean diameter of 33.5, 32.5, and 35.2 nm for blank nanoparticles, nanoconstruct **6**, **5**, and **7**. The SEM

demonstrated that the NPs are uniform and monodisperse, with a mean diameter of ~25 nm (see supplemental).

For PDT, porous nanoparticles are advantageous since release of PS from the NP is not required for the singlet oxygen to diffuse into the tumor cells. However, if the release profile is rapid the NP may not be able to efficiently deliver a high payload of the desired agent to tumor. Therefore, we investigated the release profiles of the photosensitizer **1** and the cyanine dye **3** from nanoconstructs **5–10**, respectively, by incubating them in 1% human serum albumin (HSA) at variable time points. The release profiles are summarized in the supplemental section. The release of PS **1** in nanoconstruct **6** showed a two-phase release, where an increase in the release was seen in the first four hours, which subsequently decreased during the following 20 hours. Compared to nanoconstructs **7–10**, nanoconstruct **6** showed the highest retention of PS **1** (HPPH) over a 24 hour time period with approximately 87% being retained. When comparing the percentage of PS **1** retained (at the initial time point, time zero), upon addition of 1% HSA, the nanoconstruct **8** and **10** showed the highest retention (~84 %) of the PS. To mimic the release of PS **1** and cyanine dye **3** from nanoconstruct **7** *in vivo*, the nanoformulation **7**, which provided the best whole-body fluorescence imaging and PDT response, was also subjected for the release of both the chromophores in 25% bovine calf serum (BCS, 37°C) at 4, 8, 12, and 24 hours post-addition. The maximum release (3.2%) for PS **1** occurred at 4 h time point, whereas for the cyanine dye **3**, the maximum release (2.8%) was observed at 8 h time point. These results were interesting to show a slower release of both the cyanine dye and the PS under physiologically relevant conditions.

Fluorescence imaging ability of various formulations

To show that cyanine dye **2** (IR-820, Aldrich) has poor tumor selectivity, whole body fluorescence imaging of BALB/c mice bearing subcutaneous Colon 26 tumors was performed. The water insoluble fluorophore **2** was formulated in a 1% Tween-80 / 5% dextrose solution and was injected *i.v.* at a dose of 0.3 $\mu\text{mole/kg}$. The mice were imaged at 24, 48, and 72 hours post-injection (Figure 2 B-D). Due to the rather poor tumor localization of **2**, we post-loaded it into PAA NPs formulation **4** and compared their tumor uptake and fluorescence imaging abilities. The results summarized in Figure 2 clearly indicate much improved tumor selectivity of the PAA NP formulation **4** over the free fluorophore **2**. Under similar imaging parameters, modified cyanine dye **3** and the corresponding nanoconstruct **5** (cyanine dye **3** post-loaded to PAA NPs) were also imaged (Figure 2). As can be seen, compared to cyanine dye **2** (Figure 2), the modified version **3** showed higher uptake and improved tumor-imaging ability (Figure 2, J-L). Upon post-loading the cyanine dye **3** to PAA NPs, its uptake and tumor-imaging ability at 24, 48 and 72 hours post-injection was further enhanced (Figure 3 N-P) with the difference in intensity in the tumor for **5** being statistically higher ($p < 0.05$) at 24 hours post-injection. We then decided to investigate further the utility of these biodegradable nanoparticles in developing a “multifunctional” nanoplatform. The fluorescence imaging of PAA nanoconstructs/formulations **7–10** in which HPPH **1** and cyanine dye **3** were post-loaded at a ratio of 2:1 and 4:1 (either in a single nanoparticle **7** and **8** or in separate nanoparticles **9** and **10**), respectively, was investigated in BALB/c mice bearing Colon 26 tumors. On comparing the images obtained by using the cyanine dye **3** alone and the corresponding nanoconstructs **5, 7–10** the maximum accumulation in the tumor for **3** was observed at 48 h post injection (Figure 2K), whereas the nanoconstructs produced the maximum tumor uptake at 24h post-injection (Figure 2 and 3). This could be due to a significant difference in the pharmacokinetic characteristics of the products in two different formulations. In nanoconstructs **7** and **8** in which the PS and CD were post-loaded in a ratio of 2 to 1 and 4 to 1 on excitation of the cyanine dye at 782 nm gave fluorescence at 866 and 870 nm respectively. Interestingly, both

nanoconstructs on *in vivo* excitation at 665 nm produced a significant fluorescence beyond 860 nm, which can be explained by the phenomenon known as the Förster (Fluorescence) Resonance Energy Transfer (FRET), or by the more general phenomena of energy migration, or excitation percolation, followed by energy trapping^{28,29}, analogous to the energy transport and funneling process in photosynthetic antenna. On the basis of imaging results summarized in Figure 4, the nanoconstruct **7** provided the greatest contrast between the tumor and non-tumor tissues.

Correlation between energy transfer and singlet oxygen production efficiency

It is known that when a PS is in close proximity to a longer wavelength-absorbing fluorophore, with a spectral overlap between the fluorescence of the PS and the absorbance of the fluorophore, then upon exciting the PS, the PS fluorescence decreases due to the energy transfer to the fluorophore and the singlet oxygen yield also diminishes.^{18,19} This phenomenon was evident for the nanoconstructs containing both the PS and the cyanine dye. To determine the degree of energy transfer between PS and fluorophore, the fluorescence of nanoconstructs **7** and **8** were compared with **5** and **6**. The concentration for the cyanine dye was kept constant in all nanoconstructs and the concentration of **1** for nanoconstruct **6** and **8** was kept the same and was two times higher than for nanoconstruct **7**. The fluorescence spectrum in Figure 5B shows the difference in fluorescence intensity for **6**, **7**, and **8**, which resulted from the different efficiency of the PS→CD energy transfer in these nanoconstructs. This energy transfer caused a decrease in intensity of the PS fluorescence along with an increase in CD fluorescence intensity. The energy transfer was strongest for nanoconstruct **8** since the fluorescence spectrum displayed the least intense fluorescence band from PS moiety ($\lambda_{\text{max}} \approx 670$ nm) and the most intense fluorescence band from the CD moiety ($\lambda_{\text{max}} \approx 870$ nm) upon excitation at 532 nm (Figure 5B). Also, on excitation of **3** at 785 nm, CD fluorescence was more intense for nanoconstructs **7** and **8** than for pure CD nanoconstruct **5**, even if difference in absorption at 785 nm was minimal (Figure 5C). This was an effect of the post-loaded PS molecules; their presence in the post-loaded PAA nanoparticles could result in a more dense environment for the CD molecules, which, in turn, enhanced the radiative rate for the CD fluorophore. Overall, combination of the facts that the PS fluorescence under 532 nm excitation for **7** and **8** was less intense than for **6** and, at the same time, CD fluorescence under 532 nm excitation was more intense for **7** and **8** than for **5** unambiguously demonstrates that energy transfer PS→CD occurs in nanoconstructs and its efficiency for **8** was higher than that for **7**. This higher ET efficiency can be explained by the higher concentration of PS post-loaded to nanoparticles resulting in less average distance between PS chromophores, allowing electronic excitation to migrate from one PS molecule to others, before being trapped by the CD chromophore. Lovell et al.³⁰ had reported a similar observation in a series of pyropheophorbide-*a* conjugated with quenchers. An increase in concentration of the photosensitizer possibly results in a higher probability of electronic excitation energy percolation causing the trapping of the electronic excitations by lower concentration of the quenchers (cyanine dyes).

To confirm that the more efficient PS→CD energy transfer in the nanoconstructs correlates with a less efficient production of singlet oxygen, we compared the singlet oxygen generation yield of the nanoconstructs using the singlet oxygen phosphorescence spectroscopy. Phosphorescence decays are shown in Figure 5D and demonstrate two clearly distinguishable decay rates for the singlet oxygen. One is shorter with a lifetime of ~4 s (which is close to the lifetime of singlet oxygen in water³¹) suggesting that it is derived from the excited oxygen molecules decaying in aqueous environment. The second decay rate is much longer with a lifetime of ~100 μ s, which is apparently associated with singlet oxygen decaying within the PAA matrix. The production of singlet oxygen was highest for the PS only formulation (nanoconstruct **6**) and decreases for three others in the order of **8**>**7**>**5**. We

assume that the production of singlet oxygen by **5** was negligible since it does not contain PS; thus the decay curve for **5** practically depicts the Instrument Response Function of the setup. These results were understandable since there was twice the amount of PS in nanoconstruct **8** which should produce more singlet oxygen, even if energy transfer from PS is more efficient in **8** than in **7**. Overall, it is important to stress that both **8** and **7** nanoconstructs showed singlet oxygen production comparable with that from the PS nanoparticle formulation, nanoconstruct **6**. These and our current results demonstrate that in a two-chromophore system, an increase in FRET and/or energy percolation increases the fluorescence intensity of the acceptor or longer wavelength (lower energy) chromophore, which decreases singlet oxygen production.^{18,19}

Comparative in vivo PDT efficacy of PAA NPs containing HPPH and CD in variable ratios (Nanoconstructs 6 – 10 vs. PS 1)

HPPH, derived from chlorophyll-a, is an effective PDT agent with low skin phototoxicity and, in BALB/c mice bearing Colon 26 tumors, a complete PDT response of 40% was observed at a dose of 0.47 moles/kg on exposing the tumors with light at 665 nm, delivered at a fluence and fluence-rate of 135 J/cm² and 75 mW/cm² 24 hours post-injection. To compare the newly developed nanoconstructs with free HPPH, we used similar treatment parameters as described above. In preliminary screening, the PDT response (no tumor regrowth) for HPPH **1**, nanoconstructs **6**, **7**, **8**, **9** and **10** was 40%, 40%, 60%, 30%, 40%, and 30%, respectively. The nanoconstruct **7** containing HPPH and cyanine dye **3** in a ratio of 2-1 was more effective than PS **1** alone in 1% Tween 80 formulation and nanoformulations **9** and **10**, and also provided (i) the ability to both image and treat the tumors, which could be extremely useful for a “See and Treat” approach and (ii) compared to the synthetic HPPH-cyanine dye conjugate in which the imaging dose was 8- to 10-fold lower than the therapeutic dose, a single dose (0.47 μmoles/kg) of nanoconstruct **7** can be used for both tumor imaging and PDT. T

Discussion

In our hands, compared to encapsulation,²³ the post-loading approach was more effective when hydrophobic compounds were used in conjunction with PAA nanoparticles. PAA NPs provide a great platform for post-loading because of the porous nature of the polyacrylamide-based hydrogels, wherein the hydrophobic part of the molecule may interact preferentially. We have found that the surfactant Tween-80 plays an important role in efficient retention of the compounds within the NPs. Its presence in an aqueous solution apparently causes formation of a micellar layer on the nanoconstruct surface whereby the polyethers form the outer hydrophobic layer and the oleic acid forms the inner, more hydrophobic layer of the construct.

Among all organic NIR fluorophores, cyanine dyes in general have shown great potential for fluorescence imaging.²⁵ In this series of compounds, IR-820, a near-infrared (NIR) cyanine dye, is of particular interest due to its inherent desirable photophysical characteristics, namely excitation and emission in the NIR range beyond 750 nm, which allows for deeper tissue penetration of activating light; however, its tumor uptake is known to be low.

Burns et al., have shown that when Cy5 was encapsulated within PEG-coated silica nanoparticles (3.3 and 6.0 nm diameter, respectively), the fluorescence intensity of the dye increased by 2.0 – 2.5 times, compared to that of the free dye.²⁷ This prompted us to investigate the utility of PAA nanoconstructs for the delivery of both imaging and therapeutic agents. We found that the newly constructed nanoparticles were capable of delivering a high payload of both the PS and the CD molecules to the tumor. This is likely due to the “Enhanced Permeability and Retention” (EPR) effect.^{21a,b}

The UV-Visible and fluorescence spectrometry studies confirmed that both hydrophobic PS and hydrophilic fluorophores related to cyanine dyes can be co-loaded into amine functionalized PAA nanoconstructs and maintain their photophysical characteristics. The DLS and SEM images show that upon co-post-loading, the diameter and spherical shape of the NPs remain intact. The *in vitro* spectroscopic measurements show that excitation of nanoconstruct **8** channels more energy transport/FRET from HPPH to cyanine dye **7**, resulting in reduced efficiency of **1** for PDT efficacy. In contrast to synthetic HPPH-cyanine dye conjugates, a single dose of the PAA nanoconstruct can be used simultaneously for tumor imaging and for efficient long-term tumor cure by PDT. Additionally, nanoconstructs **9** and **10** produced lower *in vivo* FRET signal as compared to nanoconstructs **7** and **8**, however the nanoconstruct **7** still provided the best PDT outcome (60% for PS **1** vs. 40% for nanoconstruct **6**). Further studies to improve the target-specificity of the nanoconstructs by introducing certain target-specific agents at the periphery of the PAA NPs are in progress.²⁶

Supplementary Material

Refer to Web version on PubMed Central for supplementary material.

Acknowledgments

The authors thank Dr. Arindam Sen, RPCI for helpful discussions and allowing us to use his research facility for determining the size of the nanoparticles.

Funding: NIH grant CA119358 and the shared resources of the Roswell Park Cancer Center support grant CA16056.

References

1. Brown SB, Brown EA, Walker I. The present and future role of photodynamic therapy in cancer treatment. *Lancet Oncol.* 2004; 5:497–508. [PubMed: 15288239]
2. Chen B, Pogue BW, Luna JM, Hardman RL, Hoopes PJ, Hasan T. Tumor vascular permeabilization by vascular-targeting photosensitization: effects, mechanism, and therapeutic implications. *Clin Cancer Res.* 2006; 12:917–923. [PubMed: 16467106]
3. Dougherty TJ, Gomer CJ, Henderson BW, Jori G, Kessel D, Korbek M, et al. Photodynamic therapy. *J Natl Cancer Inst.* 1998; 90:889–905. [PubMed: 9637138]
4. Dolmans DE, Fukumura D, Jain RK. Photodynamic therapy for cancer. *Nat Rev Cancer.* 2003; 3:380–387. [PubMed: 12724736]
5. Biel M. Advances in photodynamic therapy for the treatment of head and neck cancers. *Lasers Surg Med.* 2006; 38:349–355. [PubMed: 16788923]
6. Henderson, BW.; Gollnick, SO. Mechanistic principles of photodynamic therapy. In: Vo-Dinh, T., editor. *Biomedical Photonics Handbook*. Boca Raton: CRC Press; 2002.
7. Korbek M, Sun J. Cancer Treatment by photodynamic therapy combined with adoptive immunotherapy using genetically altered natural killer cell line. *Int J Cancer.* 2001; 93:269–274. [PubMed: 11410876]
8. Pandey RK, Goswami LN, Chen Y, Gryshuk A, Missert JR, Oseroff A, et al. Nature: a rich source for developing multifunctional agents. Tumor-imaging and photodynamic therapy. *Lasers Surg Med.* 2006; 38:445–467. [PubMed: 16788930]
9. Pandey, RK.; James, NS.; Chen, Y.; Missert, J.; Sajjad, M. Bifunctional agents for imaging and therapy in. In: Gomer, C., editor. *Methods in Molecular Biology Vol 635, Photodynamic Therapy, Methods and Protocols Ed.* New York: Springer, Humana Press; 2010.
10. Hamlin, MR. Covalent Photosensitizer Conjugates, Part 1: Antibodies and other protein for targeted photodynamic therapy in *Advances in Photodynamic Therapy*. Hamblin, MR.; Mroz, P., editors. Boston: ARTECH HOUSE; 2008.

11. (a) Kopelman R, Philbert M, Koo YEL, Moffat BA, Reddy GR, McConville P, Hall DE, Chenevert TL, Bhojani MS, Buck SM, Rehemtulla A, Ross BD. Multifunctional nanoparticle platforms for in vivo MRI enhancement and photodynamic therapy of a rat brain cancer. *J. of Magnetism and Magnetic Materials*. 2005; 293:404–410. (b) Weissleder R. *Nature Biotechnol.* 2001; 19:316–317. [PubMed: 11283581] (c) Frangioni JV. In vivo near-infrared fluorescence imaging. *Curr. Opin. Chem. Biol.* 2003; 7:626–634. [PubMed: 14580568]
12. Pandey RK, Sumlin AB, Potter WR, Bellnier DA, Henderson BW, Constantine S, et al. Structure and Photodynamic Efficacy Among Alkyl Ether Analogues of Chlorophyll-a Derivatives. *Photochem Photobiol.* 1996; 63:194–205. [PubMed: 8787014]
13. Henderson BW, Bellnier DA, Greco WR, Sharma A, Pandey RK, Vaughan L, et al. An in vivo quantitative structure-activity relationship for a congeneric series of pyropheophorbide derivatives as photosensitizers for photodynamic therapy. *Cancer Res.* 1997; 57:4000–4007. [PubMed: 9307285]
14. Bellnier DA, Henderson BW, Pandey RK, Potter WR, Dougherty TJ. Murine pharmacokinetics and antitumor efficacy of the photodynamic sensitizer 2-[1-hexyloxyethyl]-2-devinyl pyropheophorbide-a. *J Photochem Photobiol.* 1993; 20:55–61.
15. Loewen GM, Pandey RK, Bellnier D, Henderson BW, Dougherty TJ. Endobronchial photodynamic therapy for lung cancer. *Laser Surg Med.* 2006; 38:364–370.
16. Bellnier DA, Greco WR, Nava H, Loewen GM, Oseroff AR, Dougherty TJ. Mild skin photosensitivity in cancer patients following injection of Photochlor (2-[1-hexyloxy ethyl]-2-devinyl pyropheophorbide-a; HPPH) for photodynamic therapy. *Cancer Chemother Pharmacol.* 2004; 57:40–45. [PubMed: 16001178]
17. Bellnier DA, Greco WR, Loewen GM, Oseroff AO, Pandey RK, Dougherty TJ. Population pharmacokinetics of the photodynamic therapy agent 2-[1-hexyloxyethyl]-2 devinyl pyropheophorbide-a in cancer patients. *Cancer Res.* 2003; 63:1806–1813. [PubMed: 12702566]
18. Chen Y, Gryshuk A, Achilefu S, Ohulchanskyy T, Potter W, Zhong T, et al. A novel approach to a bifunctional photosensitizer for tumor Imaging and phototherapy. *Bioconjugate Chem.* 2005; 16:1264–1274.
19. Chen Y, Ohkubo K, Zhang M, Liu W, Pandey SK, Ciesielski M, et al. Photophysical, electrochemical characteristics and cross-linking of STAT-3 protein by an efficient bifunctional agent for fluorescence image-guided photodynamic therapy. *Photochem Photobiol Sci.* 2007; 6:1257–1267. [PubMed: 18046480]
20. A Wenger Y, Schneider RJ, Reddy GR, Kopelman R, Joliet O, Philbert MA. Tissue distribution and pharmacokinetics of stable polyacrylamide nanoparticles following intravenous injection in the rat. *Toxicol Appl Pharmacol.* 2011; 251:181–190. [PubMed: 21134391] B Gao D, Xu H, Philbert MA, Kopelman R. Bioeliminable nanohydrogels for drug delivery. *Nano Lett.* 2008; 8:3320–3324. [PubMed: 18788823]
21. A Meng H, Xue M, Xia T, Ji Z, Tarn DY, Zink JJ, et al. Use of Size and a Copolymer Design Feature To Improve the Biodistribution and the Enhanced Permeability and Retention Effect of Doxorubicin-Loaded Mesoporous Silica Nanoparticles in a Murine Xenograft Tumor Model. *ACS Nano.* 2011; 5:4131–4144. [PubMed: 21524062] B Matsumura Y, Maeda H. A new concept for macromolecular therapeutics in cancer chemotherapy: mechanism of tumorotropic accumulation of proteins and the antitumor agent smancs. *Cancer Res.* 1986; 46:6387–6392. [PubMed: 2946403]
22. Nasongkla N, Bey E, Ren J, Ai H, Khemtong C, Guthi JS, et al. Multifunctional polymeric micelles as cancer-targeted, MRI-ultrasensitive drug delivery systems. *Nano Lett.* 2006; 6:2427–2430. [PubMed: 17090068]
23. Wang S, Fan W, Kim G, Hah HJ, Lee YEK, Kopelman R, et al. Novel Methods to Incorporate Photosensitizers into Nanocarriers for Cancer Treatment by Photodynamic Therapy. *Lasers Surg Med.* 2011; 43:686–695. [PubMed: 22057496]
24. Thurber GM, Figuiredo JL, Weissleder R. Detection limits of intraoperative near infrared imaging for tumor resection. *J Surg Oncol.* 2010; 102:758–764. [PubMed: 20872807]
25. Rao J, Dragulescu-Andrasi A, Yao H. Fluorescence imaging in vivo: recent advances. *Curr Opin Biotechnol.* 2007; 18:17–25. [PubMed: 17234399]

26. Winer I, Wang S, Lee YEK, Fan W, Gong Y, Burgos-Ojeda D, et al. F3-targeted cisplatin-hydrogel nanoparticles as an effective therapeutic that targets both murine and human ovarian tumor endothelial cells in vivo. *Cancer Res.* 2010; 70:8674–8683. [PubMed: 20959470]
27. Burns AA, Vider J, Ow H, Herz E, Penate-Medina O, Baumgart M, et al. Fluorescent silica nanoparticles with efficient urinary excretion for nanomedicine. *Nano Lett.* 2009; 9:442–448. [PubMed: 19099455]
28. Kopelman R. Exciton percolation in mixed molecular crystals and aggregates: from naphthalene to photosynthesis. *J Phys Chem.* 1976; 80:2191–2195.
29. Hoshen J, Kopelman R. Exciton percolation I. Migration dynamics. *J Chem Phys.* 1976; 65:2817–2823.
30. Lovell JF, Chen J, Jarvi MT, Cao W-G, Allen AD, Liu Y, et al. FRET quenching of photosensitizer singlet oxygen generation. *J Phys Chem B.* 2009; 113:3203–3211. [PubMed: 19708269]
31. Ohulchanskyy T, Roy I, Goswami LN, Bergey EJ, Pandey RK, Oseroff AR, et al. Organically modified silica nanoparticles with covalently incorporated photosensitizer for photodynamic therapy of cancer. *Nano Lett.* 2007; 7:2835–2842. [PubMed: 17718587]

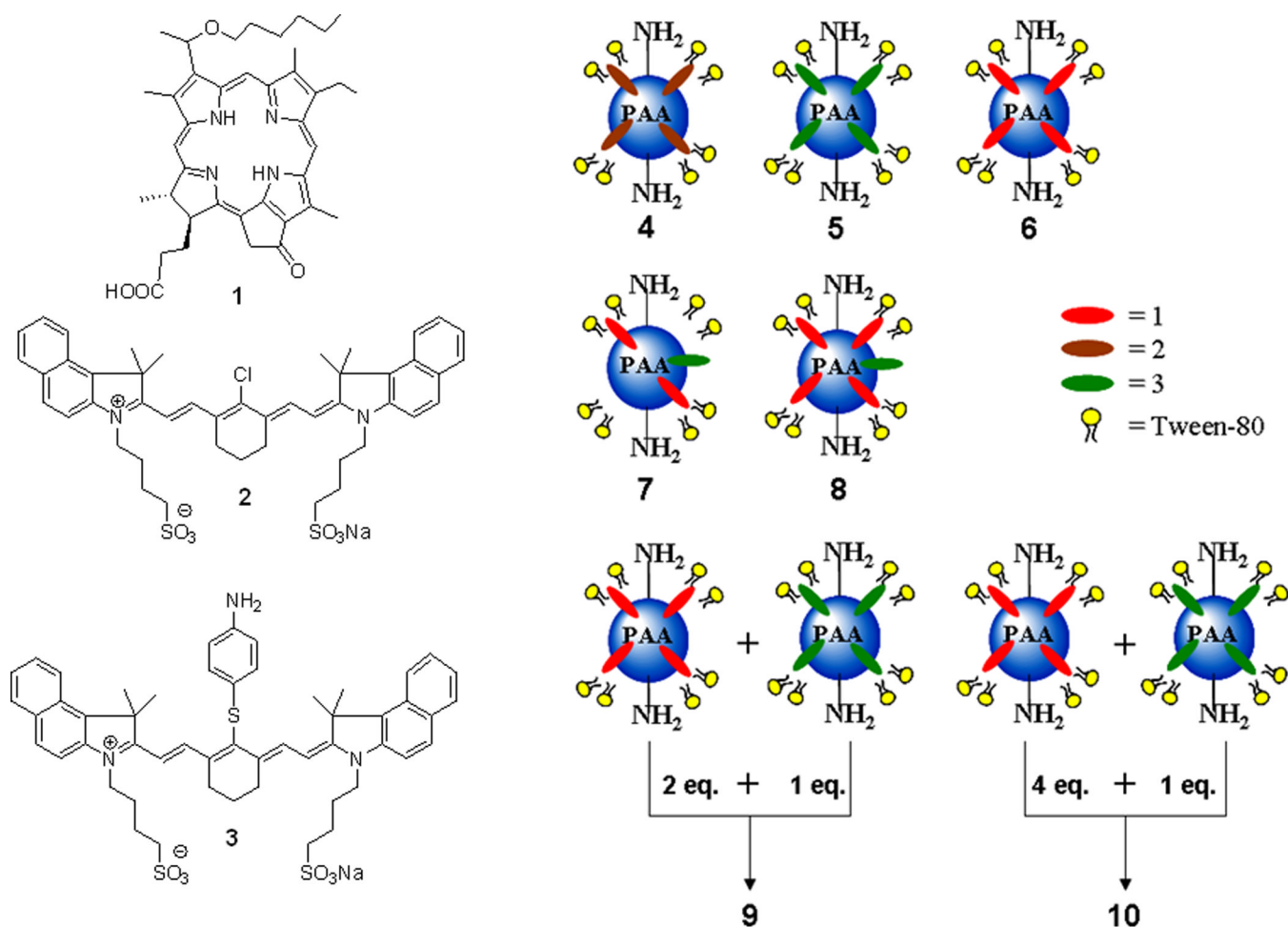


Figure 1.

Post-loading of amine functionalized PAA NPs with IR-820, cyanine dye 2: nanoconstruct 4; cyanine dye 3: nanoconstruct 5; HPPH, photosensitizer 1: nanoconstruct 6; 1 and 3 at a 2:1 molar ratio: nanoconstruct 7; and 1 and 3 at a 4:1 molar ratio: nanoconstruct 8.

Nanoformulation 9 and 10 is nanoconstruct 6 and 5 mixed such that the molar ratio of 1 to 3 is 2:1 and 4:1, respectively.

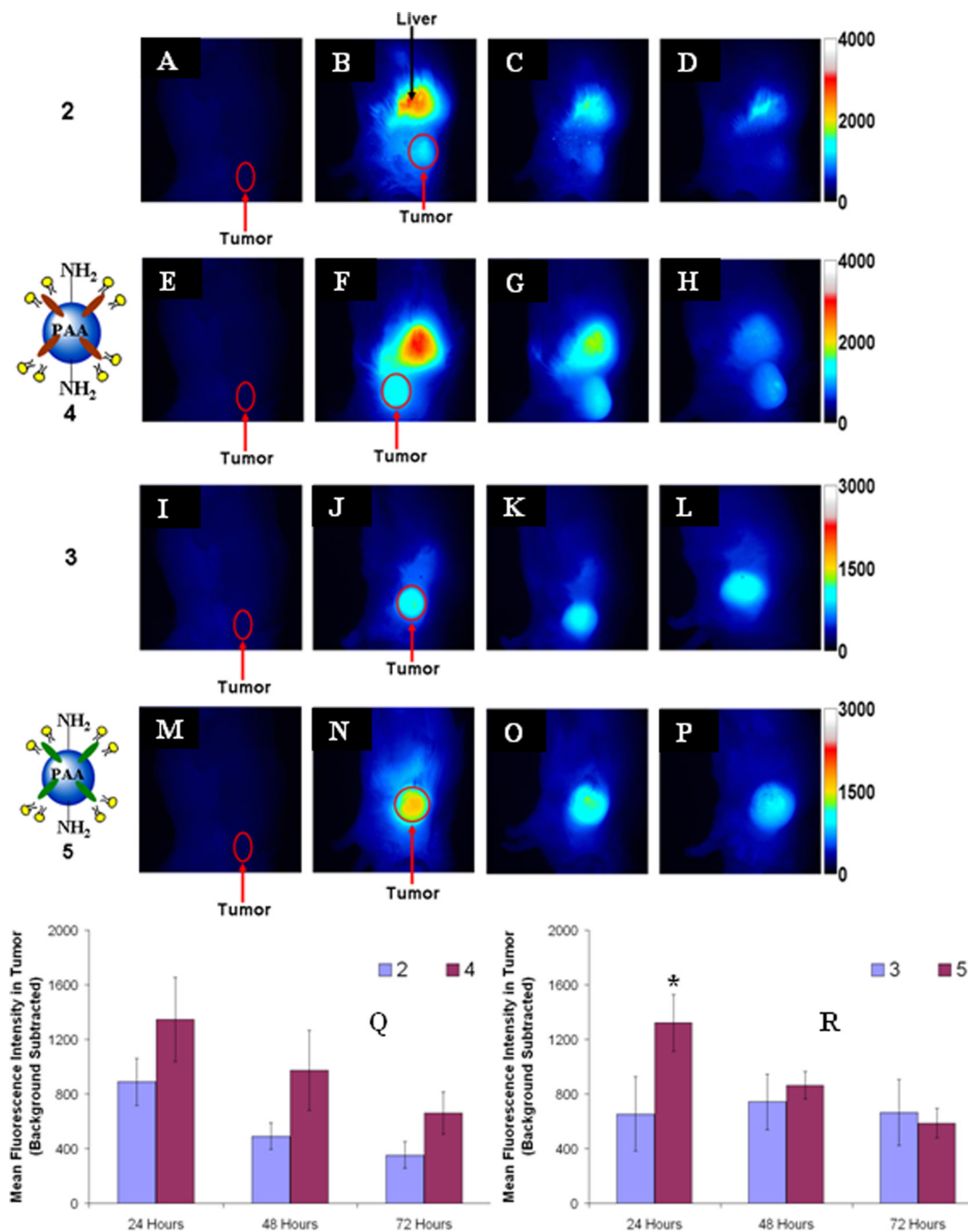


Figure 2. Whole body fluorescence images of BALB/c mice bearing Colon-26 tumors. Control mouse (A, E, I, and M), cyanine dye 2 (B-D), nanoconstruct 4 (F-H), cyanine dye 3 (J-L), nanoconstruct 5 (N-P), 24, 48, and 72h post *i.v.* injection. The fluorescence intensity values are background subtracted from the control mouse (cyanine dye 2, Q, and cyanine dye 3, R). The error bar is the standard deviation of the mean fluorescence intensity in the tumors, $n = 3$. * = statistical significance of the difference in mean fluorescence intensity ($P < 0.05$, student t-test).

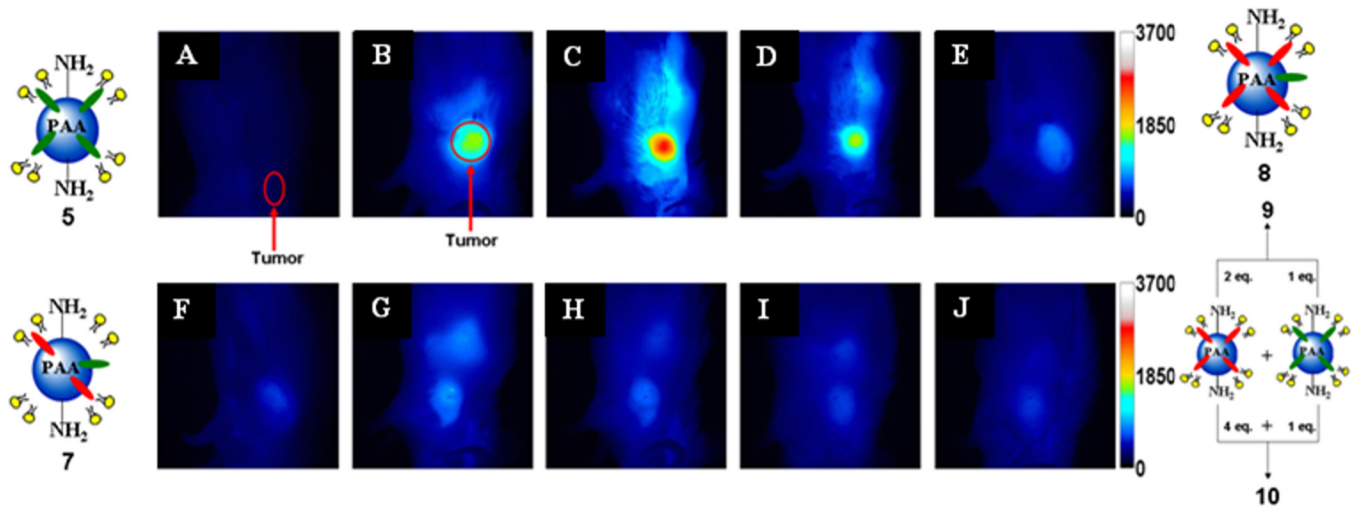
Whole-Body Fluorescence Imaging (λ_{ex} : 782 nm and λ_{em} : > 830 nm)

Figure 3. Whole body fluorescence images of a control mouse (A), nanoconstructs/formulation **5** (B), **7** (C & D), **8** (E & F), **9** (G & H) and **10** (I & J) in BALB/c mice bearing Colon-26 tumors. For A-J the excitation wavelength was 782 nm. Images A, B, C, E, G, & I and D, F, H, & J were taken 24 and 48 hours post *i.v.* injection, respectively.

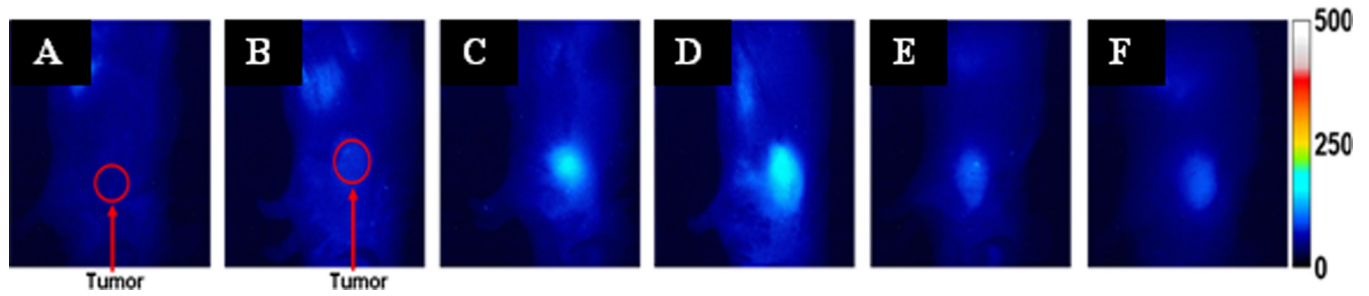
Whole-Body FRET Imaging (λ_{ex} : 665 nm and λ_{em} : > 830 nm)

Figure 4. Whole body FRET images of a control mouse (A), nanoconstructs/formulation **5** (B), **7** (C), **8** (D), **9** (E) and **10** (F) in BALB/c mice bearing Colon-26 tumors. For A-F the excitation wavelength was 665 nm. Images A-F were taken 24 hours post *i.v.* injection.

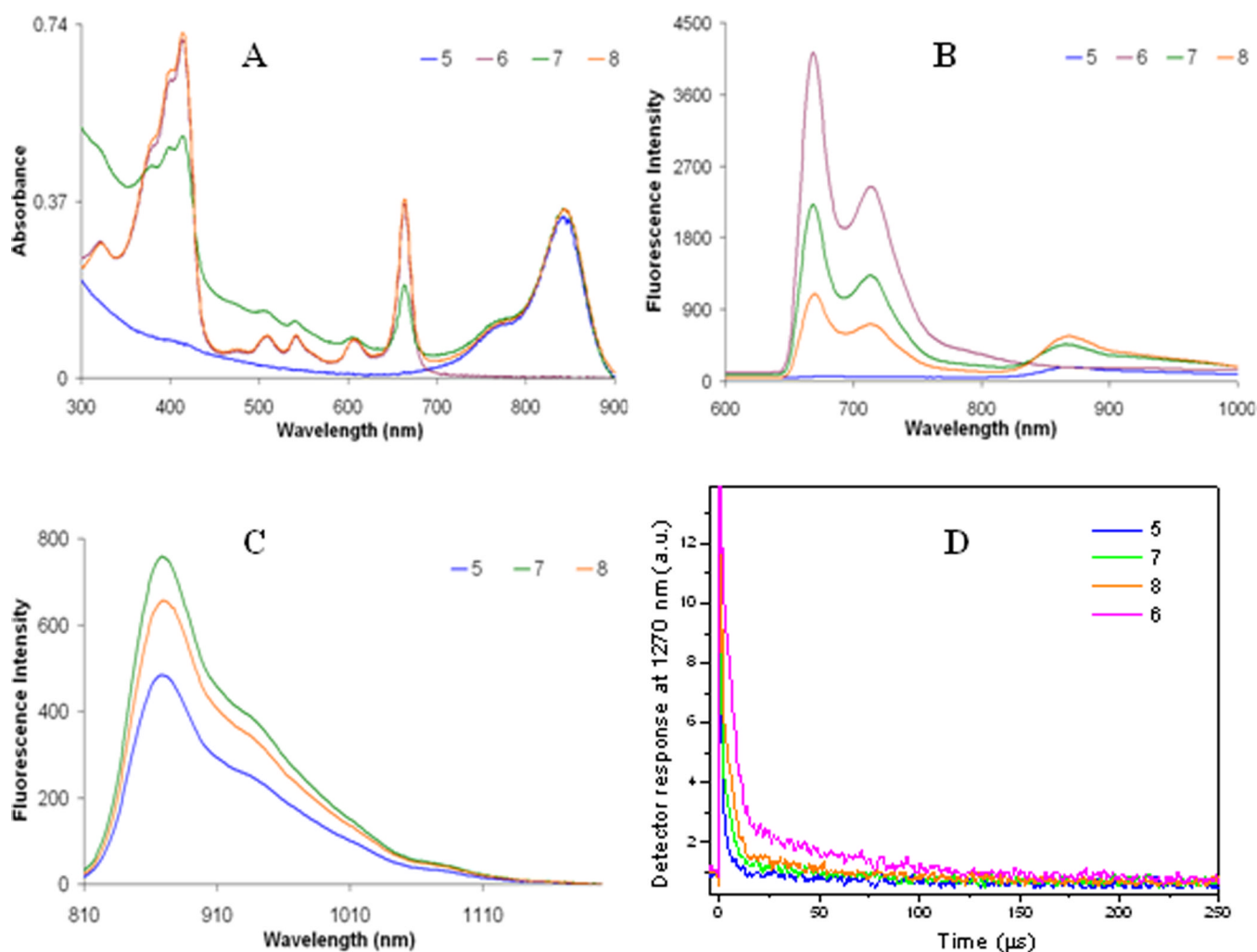


Figure 5.

A) Electronic absorption spectra of nanoconstructs **5**, **6**, **7**, and **8** in water. B) Fluorescence emission of nanoconstructs **5**, **6**, **7**, and **8** excited at 532 nm in water. C) Fluorescence emission of nanoconstructs **5**, **7**, and **8** excited at 785 nm. D) The singlet oxygen production of nanoconstructs **5**, **6**, **7**, and **8** in water was detected by measuring the phosphorescence of singlet oxygen, $^1\text{O}_2$, at 1270 nm upon excitation by a 532 nm laser. Nanoconstruct **5** was used as the instrument response function (IRF) as it does not produce $^1\text{O}_2$.

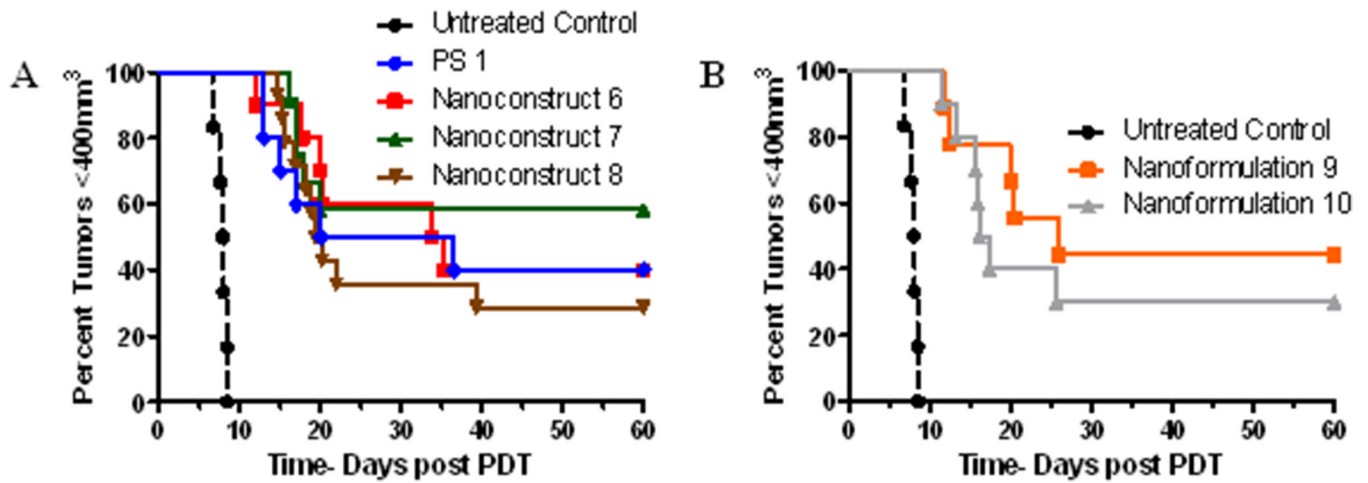


Figure 6.

Kaplan-Meier plots for BALB/c mice bearing subcutaneous Colon-26 tumors treated with PS 1 and various nanoconstructs at the PS dose of $0.47 \mu\text{mol/kg}$. The tumors were exposed to light at the light fluence and fluence rate of $135 \text{ J/cm}^2 @ 75 \text{ mW/cm}^2$. Under same treatment parameters nanoconstruct 7 (containing HPPH and CD in a ratio of 2:1) showed the best long term PDT efficacy (6/10 mice were tumor-free on day 60).